applied sciences

MDPI

Article

Potential of RCCI Series Hybrid Vehicle Architecture to Meet the Future CO_2 Targets with Low Engine-Out Emissions

Jesús Benajes, Antonio García, Javier Monsalve-Serrano * and Rafael Sari

CMT-Motores Térmicos, Universitat Politècnica de València, Camino de Vera s/n, 46022 Valencia, Spain; jbenajes@mot.upv.es (J.B.); angarma8@mot.upv.es (A.G.); rasala@mot.upv.es (R.S.)

* Correspondence: jamonse1@mot.upv.es; Tel.: +34-963-877-659

Received: 31 July 2018; Accepted: 23 August 2018; Published: 27 August 2018

Abstract: Reactivity controlled compression ignition (RCCI) combustion has been shown to provide simultaneous ultra-low NOx and soot emissions with similar or better thermal efficiencies than conventional diesel combustion (CDC). Nonetheless, RCCI still has several challenges that restrict its operating range and limit its practical application. The dual-mode operation, which involves switching between different combustion modes, has been found as a promising alternative to operation in the whole engine map. However, the combustion mode switching requires difficult engine control, particularly during transient operation. The series hybrid vehicle (SHV) architecture allows the thermal engine to operate in a limited operating range by decoupling it from the drivetrain. Therefore, it could be an interesting alternative to the dual-mode concept. This work explores the potential of the RCCI series hybrid vehicle architecture to provide low engine-out emissions and CO_2 by means of vehicle systems simulations. The results show the influence of the main parameters and control strategies of the SHV vehicle on its efficiency and emissions under different driving cycles. Finally, the optimal RCCI-SHV configuration is compared to CDC and dual-mode combustion strategies, confirming its potential as a future vehicle architecture for high efficiency and low emissions.

Keywords: reactivity controlled compression ignition; series hybrid vehicle; dual-fuel combustion; efficiency; driving cycles

1. Introduction

The future requirements regarding engine-out emissions and greenhouse gas (GHG) pollutants have been encouraging both engine original equipment manufacturers (OEMs) and the scientific community to search for alternative solutions to meet the normative constraints. Advances have been made in several systems such as injection devices (higher pressure pumps and faster injectors), combustion chamber geometry, and after-treatment devices. In parallel, new combustion modes are being developed aiming to reduce some of the raw emissions at a normative level. Among these combustion modes, the so-called low-temperature combustion (LTC) is receiving particular attention as this strategy can directly reduce the needs regarding after-treatment devices. This has fundamental importance, as these systems make up a large part of the final cost of the vehicle. The most expensive after-treatment system for vehicles operating with conventional diesel combustion is the selective catalytic reduction (SCR), which is used to reduce the levels of NOx emissions at the tailpipe. The second most expensive after-treatment system is the diesel particulate filter (DPF), which is needed to retain and oxidize the soot emissions before emission to the atmosphere. Finally, with a minor cost, a diesel oxidation catalyst (DOC) is needed to reduce the hydrocarbons (HC) and carbon monoxide (CO) emissions [1].

The major claim of the LTC concepts is the possibility to avoid the NOx-soot trade-off that occurs with conventional diesel combustion (CDC) [2] while simultaneously providing a high thermal efficiency [3]. One of the earlier investigated strategies was the homogeneous charge compression ignition (HCCI) mode. This combustion mode was able to achieve reduced NOx and soot emissions with efficiency levels similar to the diesel combustion modes. Despite these advantages, this method presented several challenges regarding combustion controllability and transient operation. In addition, its operation was limited to a narrow range due to high pressure gradients (upper limit) and excessive combustion inefficiency (lower limit). Over the years, several concepts were described in the literature such as the partially premixed combustion (PPC) [4] and spark-assisted PPC [5,6]. Nonetheless, similar issues as the one presented with HCCI combustion do not permit the attainment of a TRL (Technology Readiness Level) higher than 6 (an exception to this is the SKYACTIV engine produced by Mazda).

A recent change in the previous scenario was realized by the LTC concept called Reactivity Controlled Compression Ignition (RCCI). This concept was first presented by Inagaki et al. [7] naming it as dual-fuel premixed compression ignition (PCI) combustion. Interesting results were addressed in their research, where extremely low NOx and soot emissions together with an excellent control of the combustion onset were reported. The main hardware advance was the use of two injector systems enabling the modification of the fuel percentages. Following these findings, Kokjohn et al. [8] continued developing this concept and renamed it as RCCI [9]. As the RCCI relies on using port fuel injection (PFI) for the low reactivity fuel (LRF) and direct injection for the high reactivity fuel (HRF), additional fuel lines are needed to supply both fuels. The fuel injected by the PFI system can also enhance the volumetric efficiency by reducing the charge temperature as demonstrated in the literature [10–12]. From reviewing the literature, it can be stated that the most used HRF and LRF are diesel and gasoline, respectively [13,14]. Nonetheless, the RCCI was tested with a wide variety of fuels such as ethanol [15], methanol [16], and some others [17–20] resulting in similar results as those obtained with gasoline.

Several studies have been carried out to demonstrate the potential of the RCCI strategy addressing single-cylinder [21], multi-cylinder [22], heavy-duty [23], medium-duty [24], and light-duty diesel engines [25] operating with low [26], medium [27], and high [28] compression ratios (CR). In general, the results demonstrated that operation in stationary conditions results in NOx levels that are below the limits proposed by the emissions regulations, together with ultra-low soot emissions [29]. Despite the advantages of this combustion mode, common issues of the LTC modes are also present, such as high amounts of unburned HC and CO emissions during the low engine load operation [30], and excessive pressure rise rates (MPRR) and in-cylinder maximum pressure peaks (P_{max}) at high loads. Therefore, the RCCI operation is still restricted to moderate loads inside the engine map [31]. Some approaches have been investigated to overcome these issues and complete the engine map whenever the RCCI is unable to run properly. The low level of geometric and hardware modifications allow switching the combustion mode to, typically, CDC [32]. Nonetheless, such a strategy is difficult to justify from a technological standpoint. The RCCI/CDC dual mode can only be attractive to the transport industry if the fuel consumption versus single CDC and the cost of the required after-treatment systems needed to surpass the emissions regulations are reduced. For this purpose, the RCCI operation in the global engine map should be maximized [33].

Despite the improvements in the combustion area, achieving the normative values constraints is still a challenge. In this sense, electrification becomes more and more frequent in the OEMs in order to reduce the total CO_2 emitted by their fleet. Approaches such as fuel cell vehicles are also extensively investigated, demonstrating a capability to reduce the vehicle emissions to almost zero [34,35]. Detailed information can be found in [36,37]. Regarding electric vehicles, different concepts such as Mild, Series, and Parallel hybrid vehicles can be found as options in the market, and much research has been developed addressing their utilization. The use of high-efficiency cycles such as the Atkinson cycle [38] and low-temperature modes are a major research focus. Regarding the LTCs, their typical application

is found in series architecture due to the simplicity of the implementation and working points of view. Previous numerical studies demonstrated that the operation using RCCI combustion can reduce up to 9% of the total fuel consumption compared to a hybrid spark ignition (SI) engine [39]. In addition, experimental investigations demonstrated that the SHV can reach normative values for emissions by implementing appropriate design changes [40]. For this architecture, the charging strategy and the number of operating conditions used to charge the engine were found to have fundamental importance. Solouk et al. [41] stated that as the number of operating conditions is increased, better fuel consumption is achieved. However, the same authors recognized that the number of starts of the internal combustion engine during the cycle and the transition between the different operating conditions should be taken into account. As a general conclusion, all the authors state that the use of RCCI combustion in a series concept should improve the fuel consumption values. However, the conclusions regarding emissions on driving cycles are difficult to find in the literature.

The objective of this work is to evaluate the benefits of the hybrid architecture with the internal combustion engine (ICE), studying the RCCI combustion mode compared to conventional modes operating in diesel and dual-mode combustion. Experimental steady maps from fuel consumption and emissions were measured in a test bench for a high CR light-duty diesel engine (17.1:1) and are used as boundary conditions to estimate the transient performance of the vehicle. For this, two vehicle models were developed in GT-drive to evaluate the conventional and the hybrid powertrain. Values of fuel consumption as well as emissions were assessed for different driving cycles used for homologation purposes in Europe (worldwide harmonized light vehicles test cycle (WLTC) and real driving cycle (RDE)). This allows comparison of the final simulation values with the current normative values. In addition, the total emission of CO_2 for each case is presented and discussed to investigate the potential of the hybrid concept to meet the future CO_2 targets.

2. Materials and Methods

2.1. Test Cell, Fuels, and Engine Description

The single-cylinder diesel engine (SCE) used to acquire the experimental data that was subsequently utilized to perform the simulations is based on a production light-duty 1.9 L engine, the main characteristics of which are reported in Table 1. The engine has four valves driven by dual overhead cams. The production piston, with a re-entrant bowl and a geometric compression ratio of 17.1:1 was used. The swirl ratio was fixed at 1.4 to be representative of the value used in the production engine. To set the desired swirl ratio, the SCE was equipped with tangential and helical valves located in the intake port [42].

Table 1. Engine characteristics.

Engine Type	Four Stroke, Four Valves, Direct Injection
Number of cylinders [−]	1
Displacement [L]	0.477
Bore × stroke [mm]	82 × 90.4
Compression ratio [−]	17.1:1
Bowl type	Re-entrant
Rated power [kW]	27.5 @ 4000 rpm
Rated torque [Nm]	80 @ 2000–2750 rpm

Figure 1 shows the fuel injection systems used for RCCI operation, the main characteristics of which are depicted in Table 2. A centrally located solenoid direct injector (DI) was used to inject the EN590 diesel fuel into the cylinder. The fuel was supplied to the injector by means of a common-rail fuel injection system. A DRIVVEN controller was used to manage the different injection parameters. The gasoline fuel was injected into the intake manifold by means of a port fuel injection (PFI) governed through a Genotec unit. The PFI was located 160 mm from the intake valves to avoid pooling of the

fuel. The mass flow rate of both fuels was measured using dedicated AVL 733S fuel balances (AVL LIST GmbH, Graz, Styria, Austria). Table 3 summarizes the main properties of the diesel and gasoline fuels used in this work.

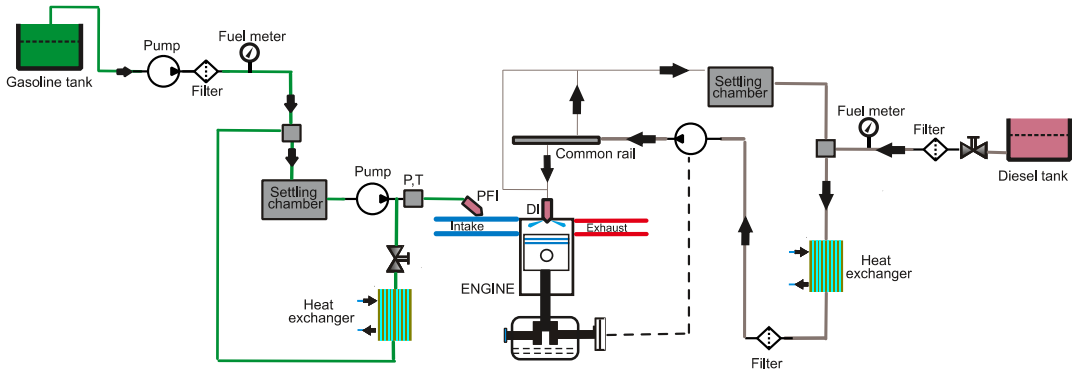

Figure 1. Fuel injection systems scheme [43]. PFI: port fuel injection; DI: direct injector.

Table 2. Diesel and gasoline fuel injector characteristics.

Diesel Injector		Gasoline Injector	
Actuation type [−]	Solenoid	Injector style [−]	Saturated
Steady flow rate @ 100 bar [cm^3/min]	880	Steady flow rate @ 3 bar [cm^3/min]	980
Included spray angle [°]	148	Included spray angle [°]	30
Number of holes [−]	7	Injection strategy [−]	single
Hole diameter [µm]	141	Start of injection [CAD aTDC]	340
Max. injection pressure [bar]	1600	Max. injection pressure [bar]	5.5

Table 3. Physical and chemical properties of the fuels.

Properties	Gasoline	Diesel
Density [kg/m^3] (T = 15 °C)	747	842
Viscosity [mm^2/s] (T = 40 °C)	0.545	2.929
Research octane number [−]	97.6	-
Motored octane number [−]	89.7	-
Cetane number [−]	-	51
Lower heating value [MJ/kg]	44.09	42.50

Figure 2 shows the layout of the test cell used in this work. During the experimental tests, the engine speed and load are controlled by an electric dynamometer. To feed the engine with fresh air, several devices are used. The first element is a screw compressor, which is used to compress the air up to a pressure of 3 bar. Afterward, a heat exchanger and an air dryer are used to set the desired temperature and relative humidity of the air. The mass air flow is measured using an airflow meter. Finally, a settling chamber is connected to the intake ducts to attenuate the pulsating flow induced by the cylinder movement. As Figure 2 shows, several pressure and temperature sensors are instrumented along the intake line to control their values. The exhaust gas recirculation (EGR) line consists of a heat exchanger to modulate the intake charge temperature, a settling chamber to promote a regular EGR mass flow, and a regulation valve to modify the EGR rate as required. As for the fresh air, the EGR temperature is controlled in various locations along the EGR line. Lastly, the temperature and pressure of the intake charge (air-EGR mixture) is controlled in the intake manifold before entering into the cylinder.

The exhaust line has a similar disposition to the intake line. First of all, the pressure and temperature of the exhaust stream are monitored through transducers located in the exhaust manifold.

After that, the flow is attenuated in a settling chamber before reaching the pneumatic valve used to regulate the EGR flow. This valve is also used to replicate the backpressure provoked by the turbine in a real engine. Finally, the emissions analyzers are located at the end of the exhaust line. The gaseous emissions are measured using a five-gas Horiba MEXA-7100 DEGR analyzer (HORIBA GmbH, Tulln, Lower Austria, Austria). Each operating point is measured three times for a period of 60 s. The smoke content of the exhaust gas is measured using an AVL 415S smoke meter (AVL LIST GmbH, Graz, Styria, Austria). In this case, each operating condition was measured three times, each sample having a volume of 1 L, with the paper-saving mode switched off. Table 4 shows the accuracy of the different elements of the test cell.

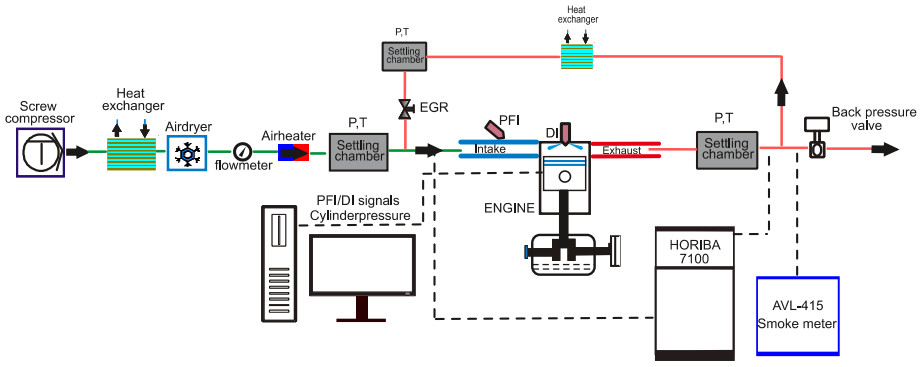

Figure 2. Test cell scheme [43]. EGR: exhaust gas recirculation.

Table 4. Accuracy of the instrumentation used in this work.

Variable	Device	Manufacturer/Model	Accuracy
In-cylinder pressure	Piezoelectric transducer	Kistler/6125BC	±1.25 bar
Intake/exhaust pressure	Piezoresistive transducers	Kistler/4603B10	±25 mbar
Temperature in settling chambers and manifolds	Thermocouple	TC direct/type K	±2.5 °C
Crank angle, engine speed	Encoder	AVL/364	±0.02 CAD
NOx, CO, HC, O_2, CO_2	Gas analyzer	HORIBA/MEXA 7100 DEGR	4%
FSN	Smoke meter	AVL/415	±0.025 FSN
Gasoline/diesel fuel mass flow	Fuel balances	AVL/733S	±0.2%
Air mass flow	Air flow meter	Elster/RVG G100	±0.1%

2.2. Mode Strategy Description and RCCI Engine Maps

The dual-mode concept combines CDC and RCCI combustion regimes to enable operation along the whole engine map. The aim of this strategy is to promote RCCI operation whenever possible and switch to CDC to cover the engine map regions in which RCCI presents difficulties. Figure 3 illustrates the dual-mode engine map proposed by the authors in a previous work [43] in which the portions covered by both combustion regimes are differentiated and the ISFC values found for the RCCI region in the map. It can be seen that the low load-low speed region of the map leads to the worst performance, while the minimum indicated specific fuel consumption (ISFC) is achieved at 3000 rpm and 7 bar indicated mean effective pressure (IMEP), with values lower than 180 g/kWh. The influence of the engine speed on the ISFC is moderate, while the engine load has a large effect The RCCI diesel-gasoline region is covered with NOx and soot emission levels below 0.4 g/kWh and 0.01 g/kWh, respectively. The maximum load achievable with RCCI was limited by excessive MPRR (>10 bar/CAD) and/or excessive in-cylinder pressure peaks (P_{max} > 160 bar). On the other hand, the lower operating region with RCCI was limited by excessive CO levels (>5000 ppm). Details regarding the dual-mode calibration procedure can be found in [31].

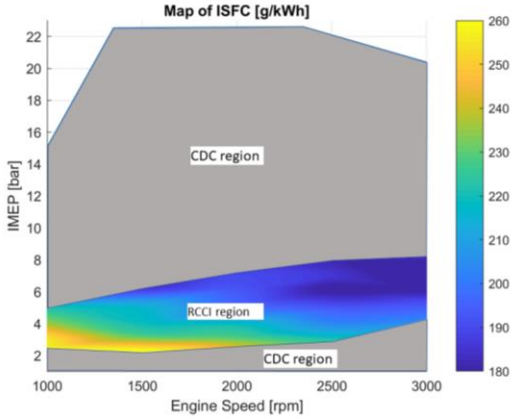

Figure 3. Illustration of the combustion strategies used to cover the engine map with the dual-mode reactivity controlled compression ignition (RCCI) diesel-gasoline/conventional diesel combustion (CDC) concept and indicated specific fuel consumption in the RCCI portion of the map. ISFC: indicated specific fuel consumption.

Figure 4 shows the engine-out emissions results for the RCCI portion of the map, which will be used to implement the RCCI-SHV configuration. In terms of engine-out emissions, it is observed that NOx emissions are below 0.4 g/kWh across the entirety of the map, and the soot emissions are an order of magnitude lower than the limit imposed during the calibration process (0.01 g/kWh). This is possible by using gasoline fraction levels from 50% to 85% over the entirety of the map [28]. Regarding HC and CO emissions, the low load region shows unacceptable levels of both pollutants, while at upper loads the HC and CO levels are approximately 8–15 g/kWh.

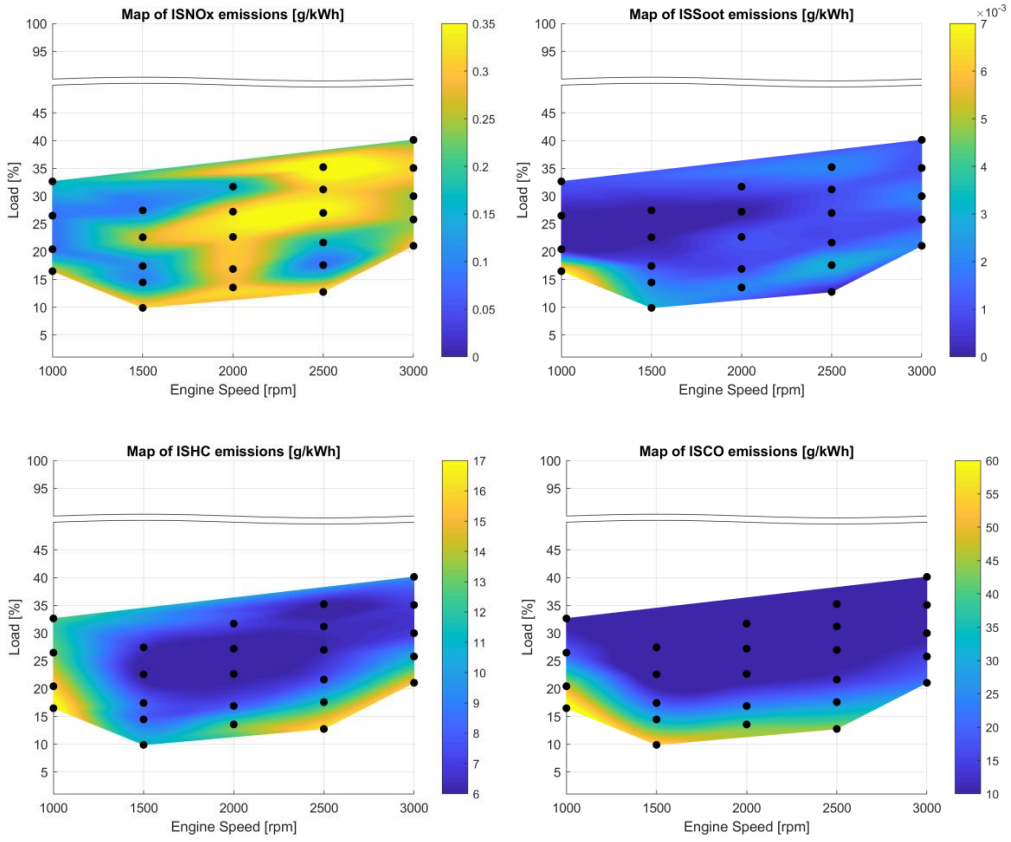

Figure 4. Engine-out emissions in the RCCI portion of the map.

2.3. Vehicle Systems and Drive-Cycle Simulations

The performance of the different concepts was assessed using the commercial software GT-Power from Gamma Technologies® (v2016, Gamma Technologies, LLC., Westmont, IL, USA, 2016). The GT-Drive package allows the simulation of the whole vehicle with its subsystem such as gearbox, tires, cooling circuits, etc. In addition, the software also possesses the required devices to perform the hybridization process, resulting in different batteries (NiMh, Li-ion, etc.), motors, and controller devices. Additionally, the vehicle can be submitted to load and speed profiles, allowing assessment of its performance on different driving cycle conditions. In this way, the mapping results from bench experiments were used as inputs for the simulation. Different models were developed for each of the powertrains, and are presented in Figure 5. The main differences between the models are the increased number of controllers, the absence of a gearbox, and the addition of batteries and motors in the hybrid powertrain system (Figure 5b).

The maps obtained from experimental bench tests are used as inputs for the model. These data are specified in the engine object in Figure 5. First, geometric parameters of the engine such as total displacement, idle, engine type, etc., are specified. Following this, the maps that characterize the workings of the engine are defined. The required maps for this step are the break mean effective pressure (BMEP) values as a function of load percentage and engine speed, and the friction mean effective pressure (FMEP) maps related to the BMEP values and the engine speed, see Figure 6. With these data, the IMEP values can be obtained, and the emissions and fuel consumption maps can be converted from indicated to brake-related values. Finally, the data for emissions and fuel consumption are inserted into the model. The advantage of this calculation method is to know, a priori, the values that the parameter will possess based on a determined operating condition (BMEP and engine speed). For intermediary conditions, the experimental maps are interpolated to predict a value. This operating condition is obtained from the solution of the differential equations of vehicular motion. The total required torque to move the vehicle is defined by Equation (1) [44].

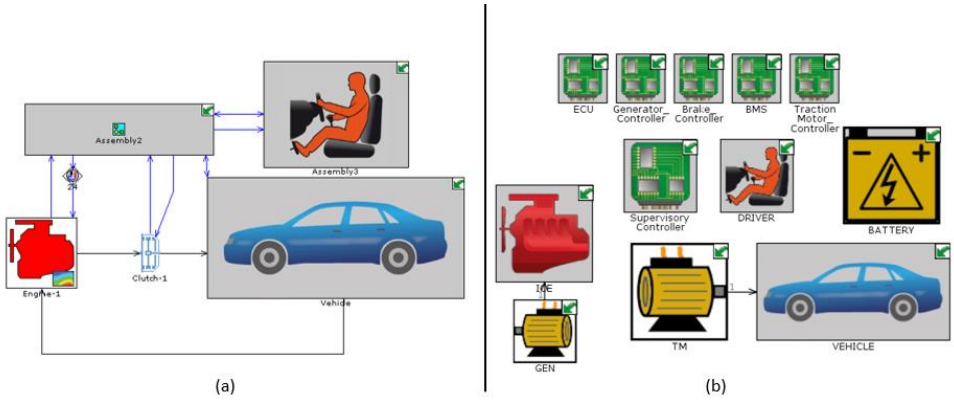

Figure 5. Simulation models built in GT-Power: (**a**) Conventional powertrain; (**b**) hybrid powertrain.

$$\tau_{vehicle} = \left[I_{trans1} + \frac{I_{trans2}}{R_t^2} + \frac{I_{dsh}}{R_t^2} + \frac{I_{axl}}{(R_d^2)(R_t^2)} + \frac{(M_{veh})(r_{whl}^2)}{(R_d^2)(R_t^2)}\right]\frac{d\omega_{drv}}{dt} - \left[\frac{I_{trans2}}{R_t^3} + \frac{I_{dsh}}{R_t^3} + \frac{I_{axl}}{(R_d^2)(R_t^3)} + \frac{(M_{veh})(r_{whl}^2)}{(R_d^2)(R_t^3)}\right]\omega_{drv}\frac{dR_t}{dt} + \left[\frac{F_{aer} + F_{rol} + F_{grd}}{R_d R_t}\right]r_{whl}. \quad (1)$$

Equation (1) relates all the forces that are acting on the vehicle to evaluate the required work to achieve the target speed. It considers parameters such as I_{trans1} and I_{trans2} (input and output inertia of the transmission system), I_{dsh} and I_{axl} (driveshaft and axle moment of inertia), R_d and R_t (terms related with the gearbox). ω_{drv} is the instantaneous vehicle speed and is a function of the wheel radius (r_{whl}).

M_{veh}, F_{aer}, F_{rol}, and F_{grd}, are the vehicle mass, aerodynamic forces, rolling resistance forces, and gravity forces respectively. For both powertrains, the same set of motion equations are solved. However, the hybrid system uses additional equations to determine the battery charging, instantaneous state of charge, etc. It is also important to mention that an additional loss term was added to the system for the hybrid powertrain. As the engine remains turned-off for long periods of time, every time it is started, an additional fuel consumption will be observed as a result of the increased heat losses. Therefore, a fuel penalty was attributed to each engine start and was considered during the simulations.

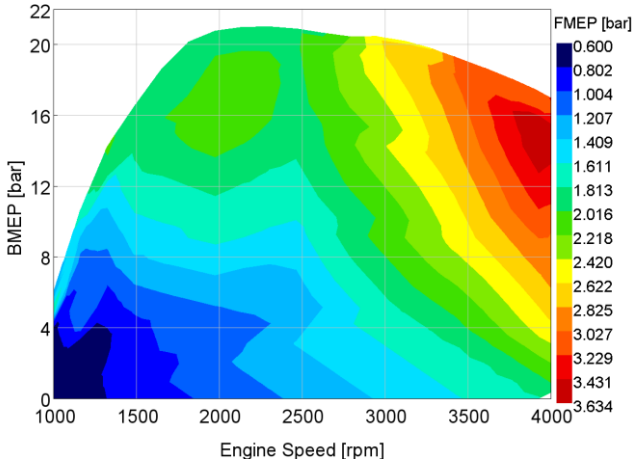

Figure 6. Friction experimental data from the engine used in this work. BMEP: break mean effective pressure.

Table 5 specifies the vehicle characteristics used in the drive-cycle simulations. The vehicle used to perform the simulations is an Opel Vectra, which is equipped with a four-cylinder engine with the same characteristics of the single-cylinder engine tested on the test bench. The aerodynamic and mechanical characterization of the vehicle allows modeling of the dragging and inertial forces that were described above.

The driving cycles selected for study in this work are the worldwide harmonized light vehicles test cycle (WLTC) and the real driving emissions cycle (RDE); chosen because they have a major relevance with regard to the current regulatory stages of the European emissions standards. The time-vehicle speed profiles for both cycles are presented in Figure 7, where the RDE profile was taken from a previous investigation made by the authors [45]. Figure 7 shows that the total duration of the WLTC cycle is 1820 s (≈23 km), while the RDE cycle has a substantially higher duration (5580 s, ≈67 km). Another important difference between both cycles is the number of accelerations and decelerations during the urban (RDE) and low (WLTC) phases. In this sense, the RDE cycle is based on real traffic conditions with a higher number of stop-starts that leads to more accelerations than the WLTC. This difference will have a direct impact on the fuel consumption and engine-out emissions.

Table 5. Vehicle specifications.

Vehicle Mass [kg]	1573
Vehicle drag coefficient [−]	0.28
Frontal area [m^2]	2.04
Tires size [mm/%/inch]	225/45/18
Additional Components for the Hybrid Powertrain	
Electric motor power [kW]	45
Generator power [kW]	25
Battery size [Ah]	20
Battery component [−]	Li-ion

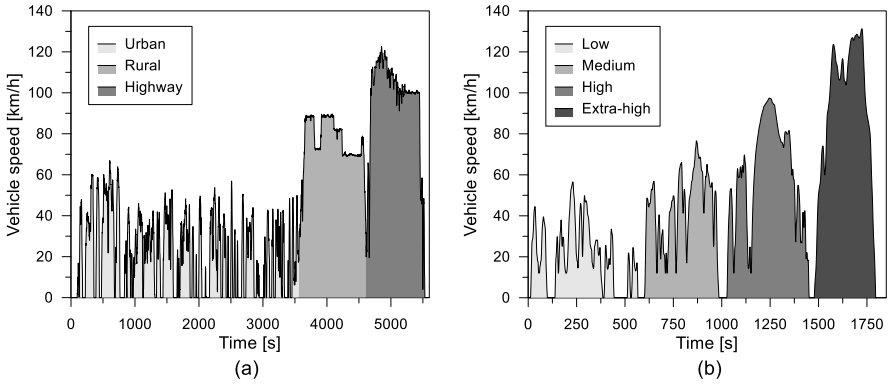

Figure 7. Time-vehicle speed profiles of the real driving emissions (RDE) (**a**) and worldwide harmonized light vehicles test cycle (WLTC) (**b**) cycles.

3. Results and Discussion

This section is divided into two subsections. The objective of the first is to find the optimal values for the state of charge (SOC) and the number of operating conditions to be run with the internal combustion engine (ICE), which is achieved through a series of parametric studies. The results are used as boundary conditions in the second subsection, where the hybrid concept is compared versus both conventional diesel combustion and dual-mode combustion.

3.1. Basic Parameters for the RCCI-SHV Operation

3.1.1. State of Charge Selection

As a preliminary study, the effect of the initial SOC on the final fuel consumption was evaluated. Four values were chosen (0.84, 0.64, 0.44 and 0.24) as initial SOC values. Its charging limits were scaled by the initial value maintaining the upper and lower limits for all the cases. Therefore, the results are function of the electrical characteristics of the vehicle, such as the charging and discharging voltage, in addition to the resistance, both functions of the actual SOC. Figure 8 shows the results obtained for the SOC sweep regarding its behavior along the driving cycle (left) and the final fuel consumption (right). As can be seen, the SOC variation is very small for the initial phases of the cycle. In these conditions, there are a considerable number of decelerations, where the brake energy recovery can take place. In addition, once the engine starts, the battery is recharged fast, because the power demand is not as high. Nonetheless, as the cycle advances towards the extra high phase, the energy demand increases, thus decreasing the SOC value. In this case, the ICE plays a key role in driving the SOC to its original level. The impact of these changes for the different initial SOCs on the final fuel consumption can be verified in Figure 8b. An absolute variation lower than 2% when comparing the two extreme values is verified. Therefore, it can be stated that, despite the variations, using initial SOC values above 0.24 returns satisfactory results.

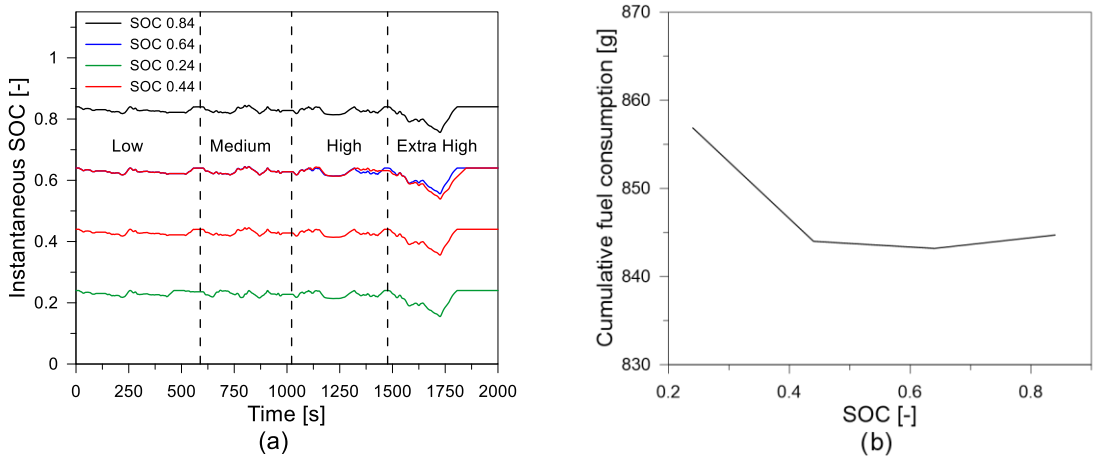

Figure 8. Instantaneous state of charge (SOC) (**a**) and final fuel consumption (**b**) for different initial SOC at the worldwide harmonized light vehicles test cycle (WLTC) driving cycle.

With the aim of verifying the influence of the driving cycle characteristics on the parametric study results, the same analysis was performed for the RDE driving cycle, as shown in Figure 9. The SOC variation along the cycle presents similar behavior to that found in the WLTC cycle, with the highest decrease in the SOC values occurring during the highway phase. Regarding the final fuel consumption, its variations for the different SOCs are close to 1%, smaller than those found with the WLTC. Again, the initial SOC of 0.24 was the one that presented the highest fuel consumption. The optimum operating range was found between 0.44 and 0.84. Therefore, an intermediate value of 0.64 was chosen as the boundary condition for the comparison against the combustion modes.

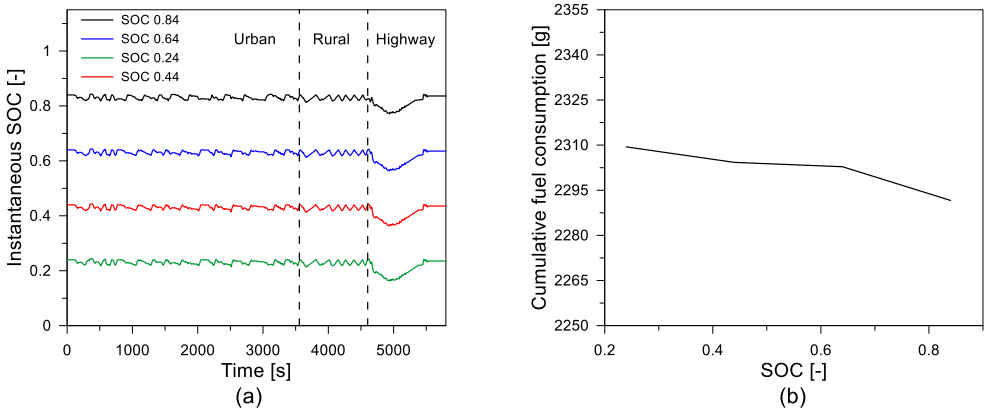

Figure 9. Instantaneous SOC (**a**) and final fuel consumption (**b**) for different initial SOC at the RDE driving cycle.

3.1.2. ICE Operating Conditions Selection

The rule-based control (RBC) charging concept relies on defining pre-established operating conditions to charge the battery whenever it is required [46]. However, the same power can be delivered by changing the total time that the engine is operating and the operating condition of the engine. As a result, the same fuel consumption will not be achieved. In addition, the battery charging can be done using a different number of operating conditions, for example, one condition of average power or two different conditions, one with lower power and the other with a higher power value. For this reason, a parametric study aiming to understand the effect of using one, two, or three operating conditions to charge the batteries was performed, which will serve to define the best strategy for the hybrid concept. All the conditions selected are inside the RCCI zone to take advantage of the benefits

in terms of efficiency, NOx, and soot emissions. The three operating conditions selected (19, 23, and 32 kW) to perform the parametric study are marked in Figure 10.

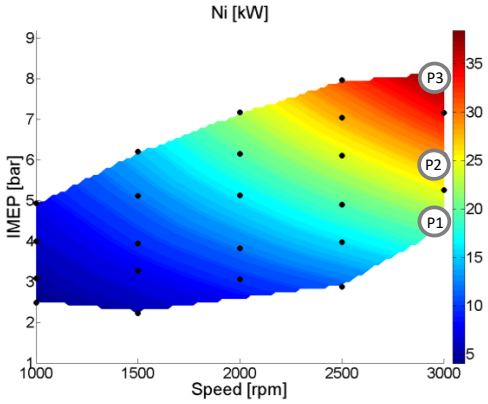

Figure 10. Indicated power in the RCCI portion of the map. The three selected points to perform the parametric study are marked in the map.

Figures 11 and 12 show the instantaneous SOC and fuel consumption along the WLTC and RDE cycle, respectively, for the cases of using one, two, or three ICE operating points. Figure 11 shows slight differences for the initial phases of the driving cycle. In these conditions, the battery is mainly charged by the energy recovered through regenerative braking, while the ICE is started during only a few intervals. After 1000 s of the cycle, the SOC profiles for the three strategies become distinct as a function of the higher power requirement. However, the great differences are observed in the highway phase, where the vehicle reaches speeds higher than 100 km/h. In this case, when three operating conditions are used, it takes a short time to recharge the battery. In addition, as the number of operating conditions is increased, the SOC variation lessened compared to the case with one operating condition. Finally, it is also seen that the use of low-power operating conditions as much as possible decreases the total mass fuel consumption as its value is proportional to the power.

Figure 12 shows similar results for the RDE driving cycle, but with lower differences in general. The only condition where it is possible to realize SOC differences is in the highway phase. For this segment, it is observed that the SOC decrease is considerably reduced as the number of operating conditions of the ICE is increased. Furthermore, the fuel consumption values also decrease for the condition with three operating points, as was found with the WLTC. Therefore, the approach based on three operating conditions to charge the battery was chosen to perform a comparative study.

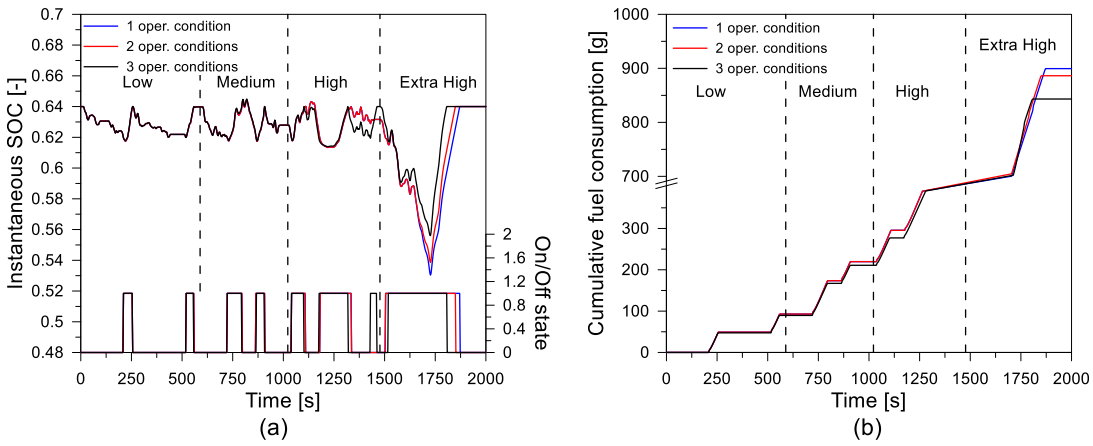

Figure 11. Instantaneous SOC (**a**) and cumulative fuel consumption (**b**) for the three-charging strategy during the WLTC driving cycle.

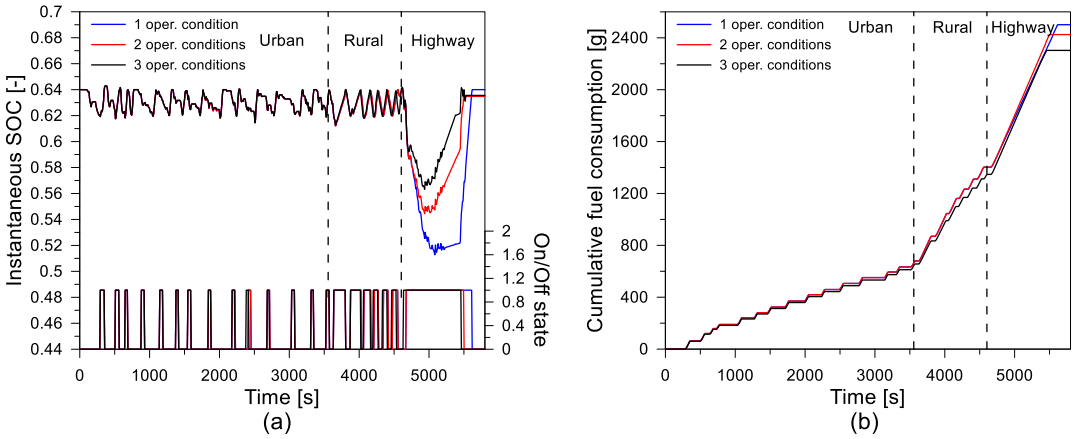

Figure 12. Instantaneous SOC (**a**) and cumulative fuel consumption (**b**) for the three-charging strategy during the real driving cycle (RDE) driving cycle.

3.2. Combustion Modes Comparison

The objective of this section is to assess the potential of the RCCI-SHV architecture compared to the dual-mode concept described in Section 2.2 and conventional diesel combustion. For this purpose, performance and emissions maps of the original diesel engine and dual-mode RCCI were used as input data for the model. The driving cycles were simulated using the same gear shifting strategy for CDC and dual-mode combustion, while the hybrid concept relied on direct transmission with a fixed gear ratio. The operating conditions reached during the RDE cycle with CDC and dual-mode concepts are shown in Figure 13. It is interesting to note that the charging strategy for the hybrid vehicle was based on RBC (rule-based control), where the engine operating conditions are defined on SOC ranges. This allows for tailoring of the operating conditions to obtain the desired values of emissions. This means that the ICE will operate in a defined operating condition based on the previous state and the actual SOC value from the battery. The basic control strategy is summarized in Table 6 where CD stands for charge depleting operation and CS for charge sustaining mode. Other control strategies such as dynamic programming and a model predictive controller are able to obtain higher energy savings, but RBC has easier implementation from the control standpoint. Therefore, the energy savings achieved with the hybrid powertrain can potentially be even higher than the values presented here. Future works will be focused on the optimization of the charging strategy.

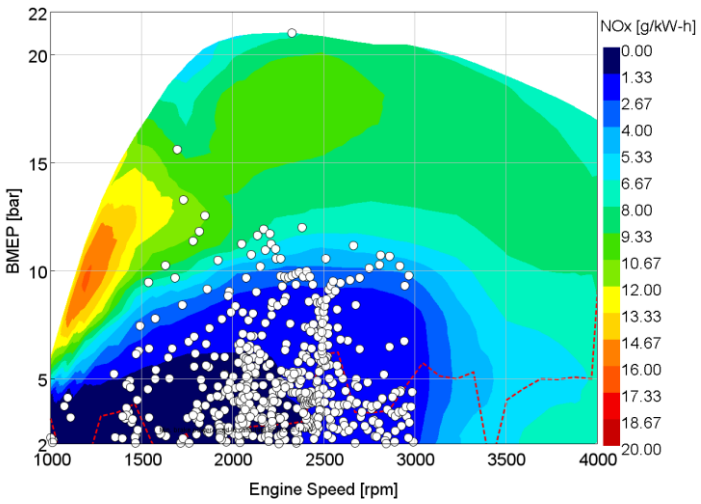

Figure 13. *Cont.*

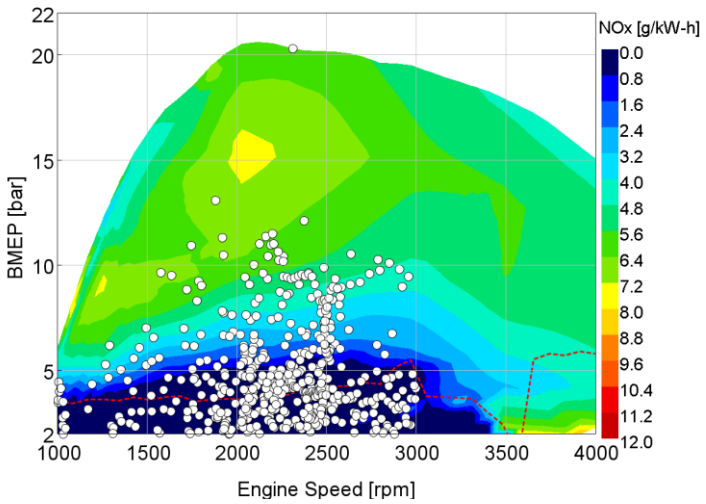

Figure 13. Operating conditions reached during the RDE cycle for CDC (**top**) and dual-mode combustion (**bottom**).

Table 6. Rule-based control (RBC) control strategy.

Transitions	Conditional Statement
CD to CS Level 1	State = 1 & SOC < 0.62
CS Level 1 to CD	State = 2 & SOC > 0.64
CS Level 1 to CS Level 2	State = 2 & SOC < 0.60
CS Level 2 to CS Level 1	State = 3 & SOC > 0.62
CS Level 2 to CS Level 3	State = 3 & SOC < 0.58
CS Level 3 to CS Level 2	State = 4 & SOC > 0.60

Figure 14 presents the results obtained for the cumulative fuel consumption and the respective fuel saving for each combustion mode. In the dual-mode case, most of the operating conditions fall inside the RCCI zone, which leads to a fuel consumption improvement of almost 5% compared to CDC. This is possible because the RCCI zone has lower values of brake-specific fuel consumption (BSFC) than CDC due to the highly diluted and fast combustion process. The RCCI-SHV strategy results in higher fuel savings since all the charging operating conditions come from the RCCI zone. In addition, the three points selected allow the ICE to run the engine in optimized conditions, overcoming the drawbacks associated with regular powertrains. The comparison with the CDC mode shows an energy saving of almost 19%. The reduction in the energy consumption is also higher compared to the dual-mode case, reaching absolute values of around 13%. Thus, despite the fact that the charging strategy is not optimal, the hybrid vehicle was able to reach considerable fuel savings compared to both RCCI and CDC operations. The values obtained for the RDE driving cycle are presented in Figure 14b. Since the RDE cycle is longer than the WLTC, the effect of the RCCI zone is observed. This is directly translated in a higher fuel saving compared to the CDC case, reaching values around 6%. Nonetheless, the same cannot be observed for the hybrid powertrain. The increased number of starts of the engine during the cycle leads to an increase in the total fuel consumption since a fuel penalty constraint was used to assess the higher fuel consumption upon starting the engine. Therefore, the final fuel saving reached 13.4%, an absolute decrease of almost 5% compared to the WLTC cycle.

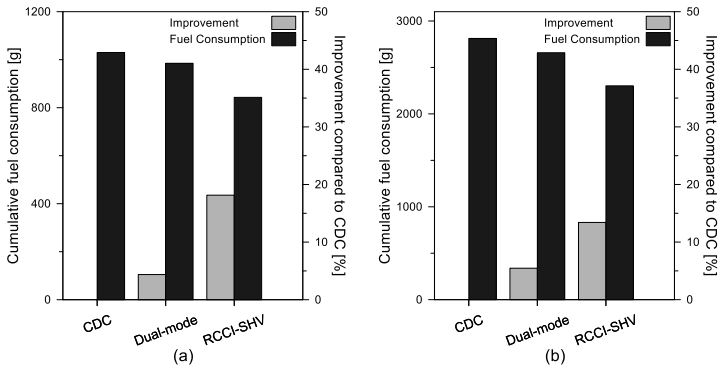

Figure 14. Cumulative fuel consumption and fuel savings for WLTC (**a**) and RDE (**b**) driving cycles.

The SOC variation during the cycle has a notable importance on the hybrid concept performance. The SOC value at the end of the cycle must reach the initial SOC to consistently deliver the same amount of energy for the driver upon each use of the car. For this study, an initial SOC value of 0.64 was used, and its behavior during the driving cycle is presented in Figure 15. It can be seen that the initial and the final values are the same. Whenever SOC reaches the lower limit, the engine starts and remains running during the time required to achieve the SOC upper limit, as illustrated by the blue line. The steady operation in a single condition defines an increasing step in the fuel consumption profile. On Figure 15b, the cumulative fuel consumption profiles during the WLTC cycle for the three modes are presented. It can be seen that the extra high phase is responsible for almost 50% of the total fuel consumption of the vehicle. In this sense, as the cycle progresses, the ICE starts to operate more frequently and at high load conditions to maintain the charge level. This can be visualized by looking at the engine state number in Figure 15a, as 1 stands for charge depleting and 4 for the higher power density condition. As a result, the extra high phase exerts a dominance on the final fuel consumption. Figure 16 shows the results of the RDE cycle. It is clear that the engine starts more frequently during this driving cycle than with the WLTC. This is directly related to the velocity profiles that were presented in Figure 7. The RDE cycle has higher velocities than the WLTC during the initial phases. Therefore, the energy requirements are also higher, making it necessary for the ICE to work. However, at the final phase of RDE, the state 4 is not achieved, i.e., the higher load condition is not required to charge the batteries. This is explained by the maximum velocity achieved during the driving cycle. While the WLTC cycle reaches maximum velocities of 130 km/h, the RDE remains under 120 km/h for the duration of the cycle. Therefore, low power density conditions are enough to maintain the charge or to drive the battery energy to its original condition.

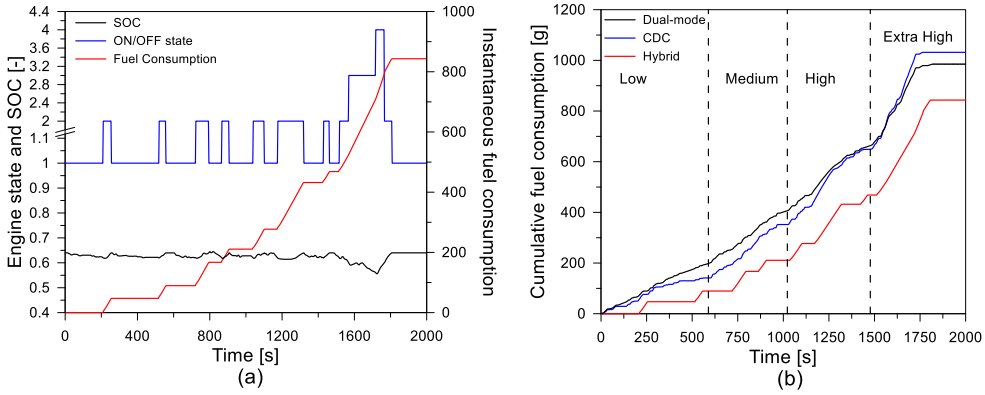

Figure 15. SOC, internal combustion engine (ICE) on-off state, and cumulative fuel consumption for the hybrid powertrain (**a**) and instantaneous fuel consumption comparison for the different concepts (**b**) during the WLTC cycle.

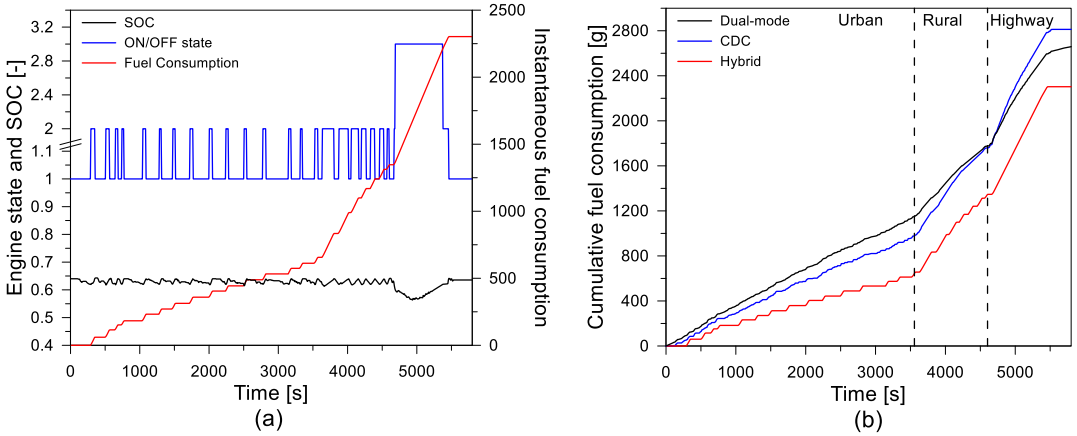

Figure 16. SOC, ICE on-off state, and cumulative fuel consumption for the hybrid powertrain (**a**) and instantaneous fuel consumption comparison for the different concepts (**b**) during the RDE cycle.

Table 6 shows the engine-out emissions for the different combustion modes and the two driving cycles. It can be seen that the dual-mode concept is not able to reach engine-out levels that are below the Euro 6 regulation levels. Therefore, it will need the conventional after-treatment layout. This is because during the driving cycles some operating conditions fall inside the CDC zone, see Figure 14, leading to an increase in the total amount of NOx and soot produced. This results in differences of NOx versus CDC of only 0.1 g/km.

In the case of the RCCI-SHV, the fixed operating conditions for the ICE allows for the best values in terms of fuel consumption and emissions to be obtained. The results confirm that the RCCI-SHV leads to the lowest engine-out emissions, with NOx and soot levels below the Euro 6 regulation. The NOx reduction versus CDC is 76.2% and 67.7% for the WLTC and RDE cycle, respectively. In terms of HC and CO, values with RCCI-SHV are higher than CDC but lower than dual-mode. However, it is expected that a conventional diesel oxidation catalyst (DOC) will reduce the RCCI-SHV tail-pipe levels below the regulation limits [47].

The CO_2 reduction is also clear from Table 7. Both concepts (dual-mode and RCCI-SHV) are able to reach consistent reductions of this pollutant, with levels below the upcoming 2021 target of 95 g/km [48]. As the RCCI concept relies on highly diluted combustion, some of the exhaust gases are recirculated to avoid high pressure gradients. Therefore, the total exhaust mass is reduced. This parameter is used to convert the concentration values of the emissions to mass flow quantities. Then, the emission values on a mass basis are considerably reduced for this combustion mode. The same can be stated for the RCCI-SHV concept, as the ICE relies on RCCI combustion. Compared to CDC, the dual-mode combustion presented a total reduction of almost 30% while the hybrid concept decreased the emissions by half, which confirms that advanced combustion modes in addition to hybrid powertrains present a huge potential to decrease the GHG emissions.

Table 7. Engine-out emissions for the different modes and the two driving cycles with the respective Euro 6 limits in g/km.

Cycle	Mode	NOx [g/km]	HC [g/km]	CO [g/km]	Soot [g/km]	CO_2 [g/km]
WLTC	CDC	0.366	0.748	1.162	0.015	132.065
	Dual-mode	0.263	1.849	5.120	0.003	95.007
	RCCI-SHV	0.078	1.138	1.726	0.001	62.292
RDE	CDC	0.256	0.944	1.451	0.013	123.606
	Dual-mode	0.165	1.806	5.105	0.002	84.591
	RCCI-SHV	0.056	1.147	1.690	0.001	60.012
Euro 6	-	0.08	0.17 *	0.5	0.005	-

* The limit for HC is a function of the total emission of NOx in Euro 6 legislation. The value of 0.17 g/km stands for the sum of HC + NOx.

4. Conclusions

This work evaluated the performance and emissions for an SHV with an ICE working under a RCCI regime and compared its values versus diesel and dual-mode combustion (diesel + RCCI). The results were obtained by means of vehicle systems simulations for the WLTC and RDE cycles. Preliminary studies demonstrated that an optimum range exists for the initial SOC of the battery (0.2 to 0.8), leading to a reduction in the final fuel consumption. This reduction can be also obtained by increasing the number of operating conditions in which the ICE works. In this sense, the use of different power conditions to charge the batteries allows the selection of the required operating condition for each driving cycle phase, improving the final performance of the vehicle.

The most important conclusions from the comparison of the three concepts (CDC, dual-mode and hybrid) under the RDE and WLTC driving cycle can be drawn as follows:

- Owing to the higher EGR levels with RCCI, lower mass flows through the exhaust system are verified for the dual-mode concept. Therefore, the total CO_2 emissions in g/km presented a decrease of almost 30% compared to the CDC case.
- The RCCI-SHV concept reduces the CO_2 emissions by half compared to the CDC case.
- The use of operating conditions calibrated to fulfill Euro 6 limits as charging points for the batteries allowed an SHV concept that presents engine-out NOx and Soot emissions inside legislation limits to be obtained without requiring DPF and SCR devices.

Therefore, it can be stated that the use of SHV in conjunction with RCCI considerably decreases the total fuel consumption of the vehicle while maintaining the NOx and soot engine-out emission levels under the Euro 6 limits. Such a result directly impacts the final after-treatment cost, since the requirements for the DPF and SCR devices can be minimized.

Author Contributions: All authors discussed and agreed on the contents of the manuscript. A.G. coordinated the experimental work defining the objectives of the tasks and guiding the technical discussion of the results and manuscript writing. J.B. provided technical guidance in experimental phases from the first stages of the project development, analyzed the results, and collaborated in the manuscript preparation. J.M.-S. and R.S. designed and performed the theoretical study and experimental tests, discussed the results, and contributed to the manuscript writing.

Funding: This research was funded by FEDER and Spanish Ministerio de Economía y Competitividad through the TRANCO project, with grant number TRA2017-87694-R.

Acknowledgments: The authors gratefully acknowledge General Motors Global Research & Development for providing the engine used to acquire the experimental data shown in this investigation.

Conflicts of Interest: The authors declare no conflict of interest. The founding sponsors had no role in the design of the study; in the collection, analyses, or interpretation of data; in the writing of the manuscript, and in the decision to publish the results.

References

1. Posada, F.; Chambliss, S.; Blumberg, K. *Costs of Emission Reduction Technologies for Heavy-Duty Diesel Vehicles*; ICCT White Paper; ICCT: Washington, DC, USA, 2016.
2. Garcia, A.; Monsalve-Serrano, J.; Heuser, B.; Jakob, M.; Kremer, F.; Pischinger, S. Influence of fuel properties on fundamental spray characteristics and soot emissions using different tailor-made fuels from biomass. *Energy Convers. Manag.* **2016**, *108*, 243–254. [CrossRef]
3. Xu, G.; Jia, M.; Li, Y.; Xie, M.; Su, W. Multi-objective optimization of the combustion of a heavy-duty diesel engine with low temperature combustion under a wide load range: (I) Computational method and optimization results. *Energy* **2017**, *126*, 707–719. [CrossRef]
4. Manente, V.; Tunestal, P.; Johansson, B.; Canella, W. *Effects of Ethanol and Different Type of Gasoline Fuels on Partially Premixed Combustion from Low to High Load*; SAE Technical Paper 2010-01-0871; SAE International: Troy, MI, USA, 2010.

5. Benajes, J.; Molina, S.; García, A.; Monsalve-Serrano, J.; Durrett, R. Performance and engine-out emissions evaluation of the double injection strategy applied to the gasoline partially premixed compression ignition spark assisted combustion concept. *Appl. Energy* **2014**, *134*, 90–101. [CrossRef]
6. Benajes, J.; Molina, S.; García, A.; Monsalve-Serrano, J.; Durrett, R. Conceptual model description of the double injection strategy applied to the gasoline partially premixed compression ignition combustion concept with spark assistance. *Appl. Energy* **2014**, *129*, 1–9. [CrossRef]
7. Inagaki, K.; Fuyuto, T.; Nishikawa, K.; Nakakita, K.; Sakata, I. *Dual-Fuel PCI Combustion Controlled by In-Cylinder Stratification of Ignitability*; SAE Technical Paper 2006-01-0028; SAE International: Troy, MI, USA, 2006.
8. Kokjohn, S.L.; Hanson, M.; Splitter, D.; Reitz, R. *Experimental Modeling of Dual-Fuel HCCI and PCCI Combustion Using In-Cylinder Fuel Blending*; SAE Technical Paper 2009-01-2647; SAE International: Troy, MI, USA, 2010.
9. Kokjohn, S.L.; Hanson, M.; Splitter, D.; Reitz, R. Fuel reactivity controlled compression ignition (RCCI): A pathway to controlled high-efficiency clean combustion. *Int. J. Engine Res.* **2011**, *12*, 209–226. [CrossRef]
10. Eyidogan, M.; Ozsezen, A.; Canakci, M.; Turkcan, A. Impact of alcohol–gasoline fuel blends on the performance and combustion characteristics of an SI engine. *Fuel* **2010**, *89*, 2713–2720. [CrossRef]
11. Vancoillie, J.; Demuynck, J.; Sileghem, L.; Van De Ginste, M.; Verhelst, S. Comparison of the renewable transportation fuels, hydrogen and methanol formed from hydrogen, with gasoline—Engine efficiency study. *Int. J. Hydrog. Energy* **2012**, *37*, 9914–9924. [CrossRef]
12. Heywood, J. *Internal Combustion Engines Fundamentals*, 1st ed.; McGraw-Hill: New York, NY, USA, 1988; pp. 1–930.
13. Li, J.; Yang, W.; Zhou, D. Review on the management of RCCI engines. *Renew. Sustain. Energy Rev.* **2017**, *69*, 65–79. [CrossRef]
14. Benajes, J.; Pastor, J.V.; García, A.; Monsalve-Serrano, J. An experimental investigation on the Influence of piston bowl geometry on RCCI performance and emissions in a heavy-duty engine. *Energy Convers. Manag.* **2015**, *103*, 1019–1030. [CrossRef]
15. Sarjovaara, T.; Larmi, M. Dual fuel diesel combustion with an E85 ethanol/gasoline blend. *Fuel* **2015**, *139*, 704–714. [CrossRef]
16. Zhou, D.; Yang, W.; An, H.; Li, J.; Shu, C. A numerical study on RCCI engine fueled by biodiesel/methanol. *Energy Convers. Manag.* **2015**, *89*, 798–807. [CrossRef]
17. Zhang, C.; Zhang, C.; Xue, L.; Li, Y. Combustion characteristics and operation range of a RCCI combustion engine fueled with direct injection n-heptane and pipe injection n-butanol. *Energy* **2017**, *125*, 439–448. [CrossRef]
18. Benajes, J.; Molina, S.; García, A.; Monsalve-Serrano, J. Effects of low reactivity fuel characteristics and blending ratio on low load RCCI (reactivity controlled compression ignition) performance and emissions in a heavy-duty diesel engine. *Energy* **2015**, *90*, 1261–1271. [CrossRef]
19. Pan, S.; Li, X.; Han, W.; Huang, Y. An experimental investigation on multi-cylinder RCCI engine fueled with 2-butanol/diesel. *Energy Convers. Manag.* **2017**, *154*, 92–101. [CrossRef]
20. Benajes, J.; Molina, S.; García, A.; Monsalve-Serrano, J. Effects of Direct injection timing and Blending Ratio on RCCI combustion with different Low Reactivity Fuels. *Energy Convers. Manag.* **2015**, *99*, 193–209. [CrossRef]
21. Li, B.; Li, Y.; Liu, H.; Liu, F.; Wang, J. Combustion and emission characteristics of diesel engine fueled with biodiesel/PODE blends. *Appl. Energy* **2017**, *206*, 425–431. [CrossRef]
22. Curran, S.; Hanson, R.; Wagner, R. Reactivity controlled compression ignition combustion on a multi-cylinder light-duty diesel engine. *Int. J. Engine Res.* **2012**, *13*, 216–225. [CrossRef]
23. Benajes, J.; García, A.; Pastor, J.M.; Monsalve-Serrano, J. Effects of piston bowl geometry on Reactivity Controlled Compression Ignition heat transfer and combustion losses at different engine loads. *Energy* **2016**, *98*, 64–77. [CrossRef]
24. Benajes, J.; García, A.; Monsalve-Serrano, J.; Balloul, I.; Pradel, G. Evaluating the reactivity controlled compression ignition operating range limits in a high-compression ratio medium-duty diesel engine fueled with biodiesel and ethanol. *Int. J. Engine Res.* **2017**, *18*, 66–80. [CrossRef]
25. Park, S.; Shin, D.; Park, J. Effect of ethanol fraction on the combustion and emission characteristics of a dimethyl ether-ethanol dual-fuel reactivity controlled compression ignition engine. *Appl. Energy* **2016**, *182*, 243–252. [CrossRef]

26. Benajes, J.; Pastor, J.V.; García, A.; Boronat, V. A RCCI operational limits assessment in a medium duty compression ignition engine using an adapted compression ratio. *Energy Convers. Manag.* **2016**, *126*, 497–508. [CrossRef]
27. Yang, B.; Yao, M.; Cheng, W.; Li, Y.; Zheng, Z.; Li, S. Experimental and numerical study on different dual-fuel combustion modes fuelled with gasoline and diesel. *Appl. Energy* **2014**, *113*, 722–733. [CrossRef]
28. Li, J.; Yang, W.; Goh, T.; An, H.; Maghbouli, A. Study on RCCI (reactivity controlled compression ignition) engine by means of statistical experimental design. *Energy* **2014**, *78*, 777–787. [CrossRef]
29. Benajes, J.; García, A.; Monsalve-Serrano, J.; Boronat, V. An investigation on the particulate number and size distributions over the whole engine map from an optimized combustion strategy combining RCCI and dual-fuel diesel-gasoline. *Energy Convers. Manag.* **2017**, *140*, 98–108. [CrossRef]
30. Desantes, J.M.; Benajes, J.; García, A.; Monsalve-Serrano, J. The Role of the In-Cylinder Gas Temperature and Oxygen Concentration over Low Load RCCI Combustion Efficiency. *Energy* **2014**, *78*, 854–868. [CrossRef]
31. Benajes, J.; García, A.; Monsalve-Serrano, J.; Villalta, D. Exploring the limits of the reactivity controlled compression ignition combustion concept in a light-duty diesel engine and the influence of the direct-injected fuel properties. *Energy Convers. Manag.* **2018**, *157*, 277–287. [CrossRef]
32. Benajes, J.; García, A.; Monsalve-Serrano, J.; Villalta, D. Benefits of E85 versus gasoline as low reactivity fuel for an automotive diesel engine operating in reactivity controlled compression ignition combustion mode. *Energy Convers. Manag.* **2018**, *159*, 85–95. [CrossRef]
33. Benajes, J.; García, A.; Monsalve-Serrano, J.; Balloul, I.; Pradel, G. An assessment of the dual-mode reactivity controlled compression ignition/conventional diesel combustion capabilities in a EURO VI medium-duty diesel engine fueled with an intermediate ethanol-gasoline blend and biodiesel. *Energy Convers. Manag.* **2016**, *123*, 381–391. [CrossRef]
34. Das, V.; Padmanaban, S.; Venkitusamy, K.; Selvamuthukumaran, R.; Blaabjerg, F.; Siano, P. Recent advances and challenges of fuel cell based power system architectures and control—A review. *Renew. Sustain. Energy Rev.* **2017**, *73*, 10–18. [CrossRef]
35. Sulaiman, N.; Hannan, M.; Mohamed, A.; Majlan, E.; Wan Daud, W. A review on energy management system for fuel cell hybrid electric vehicle: Issues and challenges. *Renew. Sustain. Energy Rev.* **2015**, *52*, 802–814. [CrossRef]
36. Shekhar, H.; Tan, C.; Yatim, A. Fuel cell hybrid electric vehicles: A review on power conditioning units and topologies. *Renew. Sustain. Energy Rev.* **2017**, *76*, 268–291.
37. Sinigaglia, T.; Lewiski, F.; Martins, M.; Siluk, J. Production, storage, fuel stations of hydrogen and its utilization in automotive applications-a review. *Int. J. Hydrog. Energy* **2017**, *42*, 24597–24611. [CrossRef]
38. Zhao, J. Research and application of over-expansion cycle (Atkinson and Miller) engines—A review. *Appl. Energy* **2017**, *185*, 300–319. [CrossRef]
39. Solouk, A.; Shakiba-herfeh, M.; Kannan, K.; Solmaz, H.; Dice, P.; Bidarvatan, M.; Kondipati, N.N.; Shahbakhti, M. *Fuel Economy Benefits of Integrating a Multi-Mode Low Temperature Combustion (LTC) Engine in a Series Extended Range Electric Powertrain*; SAE Technical Paper 2016-01-2361; SAE International: Troy, MI, USA, 2016.
40. Hanson, R.; Spannbauer, S.; Gross, C.; Reitz, R.; Curran, S.; Storey, J.; Huff, S. *Highway Fuel Economy Testing of an RCCI Series Hybrid Vehicle*; SAE Technical Paper 2015-01-0837; SAE International: Troy, MI, USA, 2015.
41. Solouk, A.; Shahbakhti, M. Energy Optimization and Fuel Economy Investifation of a Series Hybrid Elctric Vehicle Integrated with Duesel/RCCI Engines. *Energies* **2016**, *9*, 1020. [CrossRef]
42. Olmeda, P.; Martin, J.; Garcia, A.; Villalta, D.; Warey, A.; Domenech, V. A Combination of Swirl Ratio and Injection Strategy to Increase Engine Efficiency. *SAE Int. J. Engines* **2017**, *10*, 1204–1216. [CrossRef]
43. Benajes, J.; García, A.; Monsalve-Serrano, J.; Sari, R. Fuel consumption and engine-out emissions estimations of a light-duty engine running in dual-mode RCCI/CDC with different fuels and driving cycles. *Energy* **2018**, *157*, 19–30. [CrossRef]
44. GT-Suite. *Engine Performance Application Manual*; Gamma Technologies: Westmont, IL, USA, 2016.
45. Luján, J.M.; Bermúdez, V.; Dolz, V.; Monsalve-Serrano, J. An assessment of the real-world driving gaseous emissions from a Euro 6 light-duty diesel vehicle using a portable emissions measurement system (PEMS). *Atmos. Environ.* **2018**, *174*, 112–121.
46. Peng, J.; He, H.; Xiong, R. Rule based energy management strategy for a series–parallel plug-in hybrid electric bus optimized by dynamic programming. *Appl. Energy* **2015**, *185*, 1633–1643. [CrossRef]

47. European Commission. Commission Regulation (EC) No. 692/2008 of 18 July 2008 Implementing and Amending Regulation (EC) No. 715/2007 of the European Parliament and of the Council on Type-Approval of Motor Vehicles with Respect to Emissions from Light Passenger and Commercial Vehicles (Euro 5 and Euro 6) and on Access to Vehicle Repair and Maintenance Information. *Off. J. Eur. Union* **2008**, *L199*, 133–259.
48. Reducing CO_2 Emissions from Passenger Cars. European Commission Retrieved July 2018. Available online: https://ec.europa.eu/clima/policies/transport/vehicles/cars_en (accessed on 2 July 2018).